Inorganic nanotubes and fullerene-like nanoparticles

Although graphite, with its anisotropic two-dimensional lattice, is the stable form of carbon under ambient conditions, on nanometre length scales it forms zero- and one-dimensional structures, namely fullerenes and nanotubes, respectively. This virtue is not limited to carbon and, in recent years, fullerene-like structures and nanotubes have been made from numerous compounds with layered two-dimensional structures. Furthermore, crystalline and polycrystalline nanotubes of pure elements and compounds with quasi-isotropic (three-dimensional) unit cells have also been synthesized, usually by making use of solid templates. These findings open up vast opportunities for the synthesis and study of new kinds of nanostructures with properties that may differ significantly from the corresponding bulk materials. Various potential applications have been proposed for the inorganic nanotubes and the fullerene-like phases. Fullerene-like nanoparticles have been shown to exhibit excellent solid lubrication behaviour, suggesting many applications in, for example, the automotive and aerospace industries, home appliances, and recently for medical technology. Various other potential applications, in catalysis, rechargeable batteries, drug delivery, solar cells and electronics have also been proposed.

R. TENNE

Head of Department of Materials and Interfaces; Director of the Helen and Martin Kimmel Center for Nanoscale Science; holder of the Drake Family Professorial Chair in Nanotechnology, Weizmann Institute of Science, Rehovot 76100, Israel.

e-mail: reshef.tenne@weizmann.ac.il

Chemistry is, in general, not favourable of materials with empty space because the chemical bond is not stable beyond a distance of a few angstroms. Therefore, in order to maximize the interaction between the electron clouds of nearest-neighbour atoms and thereby stabilize the chemical bond between them, atoms in materials arrange themselves in close proximity. This paradigm is reflected by 'space-filling models', which visualize the overlapping electron clouds of neighbouring atoms in a given compound or a solid. Consequently, until recently, the science and technology of hollow-closed structures was in fact an almost unexplored terrain. Pauling was among the first to investigate closed polyhedral and tubular forms of asbestos minerals, such as kaolinite (alumino-silicate)[1]. Noted also for their tendency to form polyhedral structures are the boron–carbon–hydrogen compounds (carbohydrenes), which were investigated in great detail by Lipscomb[2,3].

The discovery of carbon fullerenes by Kroto, Smalley and Curl[4] in 1985 and later on carbon nanotubes by Iijima[5] served as a turning point in the exploration of this unknown territory. Perhaps equally important was the discovery of inorganic nanotubes and fullerene-like structures[6] in 1992, establishing a new paradigm in the chemistry of nanomaterials and leading to the birth of a new field of inorganic chemistry, that is, one dealing with polyhedral (closed hollow) nanostructures.

It was in fact quite natural to assume that the virtue of fullerenes and nanotubes is not limited to carbon, and could occur in other two-dimensional layered compounds, such as WS_2 (ref. 6) or its structural analogue MoS_2 (refs 7,8). In contrast to graphite, which is made of mono-atomic carbon sheets arranged in a hexagonal honeycomb and held together by van der Waals forces, these inorganic two-dimensional solids are made of stacked molecular sheets. Each molecular sheet consists of a sixfold-bonded molybdenum layer sandwiched between two threefold-bonded sulphur layers. Here too, the sheets (walls) are held together by van der Waals forces. In analogy with graphite, the unit cell of MoS_2 is made of two layers in hexagonal arrangement (2H). However, rim Mo and S atoms, which are abundant in the nano-regime, are only four- and twofold-bonded, respectively, making these nanostructures unstable in the planar form. Therefore, by folding the molecular sheet and stitching the rim atoms together, seamless stable nanotubular (one-dimensional) and spherical (zero-dimensional) structures with all Mo and S atoms being six- and threefold-bonded, respectively, are obtained. Following this early observation, nanostructures of these kinds were shown to be ubiquitous among layered compounds and were termed inorganic fullerene-like structures and inorganic nanotubes. Much like their carbon predecessors, they come in

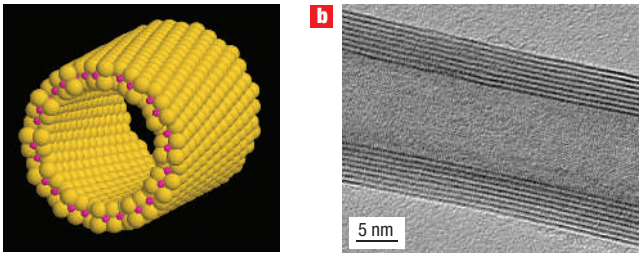

Figure 1 Presentation of WS_2 nanotubes, which are synthesized in large amounts by sulphidizing tungsten oxide nanoparticles in a fluidized bed reactor. **a**, Schematic presentation of a single-wall WS_2 nanotube with W and S atoms in pink and yellow respectively. Reproduced from ref. 76 by permission of the PCCP Owner Societies. **b**, A TEM image of a portion of a multiwall WS_2 nanotube with eight cylindrical and concentric layers. The distance between each layer is 0.61 nm. The *c* axis [001] is always normal to the surface of the nanotube.

various forms and shapes, such as multiwall and single-wall nanotubes and nested (multiwall) fullerene-like structures. Unlike carbon fullerenes and nanotubes, which can easily be synthesized in single-wall form, here, concentric (nested) multilayer structures are usually obtained. Figure 1a shows a schematic presentation of a WS_2 nanotube, and Fig. 1b shows a transmission electron microscope (TEM) image of a multiwall WS_2 nanotube.

Practically, the synthesis of pure phases of this kind proved to be relatively straightforward in several cases (MoS_2, WS_2, VO_x-alkylamine and titanate nanotubes), but exceedingly difficult if not impossible in other cases, such as that of $NiCl_2$ (ref. 9) and Cs_2O (refs 10,11). More recently, the synthesis of crystalline nanotubes from quasi-isotropic (three-dimensional) compounds, for example GaN (ref. 12) and In_2O_3 (ref. 13) was accomplished. In fact, these kind of nanotubes are not formed by the winding of a molecular sheet, but instead can be visualized as crystalline hollow nanofibres. They are usually obtained by templating and in most cases are highly faceted. Furthermore, the inner and outer surfaces of such nanotubes are generally very reactive, as can be seen, for example, by the formation of an amorphous indium oxide film on InN nanotubes[14].

Recent studies have alluded to the numerous potential applications of inorganic nanotubes and fullerene-like nanoparticles. These applications are highlighted in a recent report[15] and will be discussed in some detail below. Most importantly, fullerene-like WS_2 and MoS_2 nanoparticles were shown to exhibit superior tribological behaviour, particularly under high loads. This behaviour offers a plethora of potential applications. Various other potential applications in areas such as catalysis, energy conversion and storage, drug delivery and sensors will be discussed as well.

THE SYNTHESIS OF INORGANIC NANOTUBES AND FULLERENES

The synthesis of such nanoparticles has witnessed a substantial growth in recent years[16–20]. Therefore, this review will focus on the most recent developments, particularly those of the last three years.

The synthesis of fullerene-like structures and nanotubes of MX_2 (M=transition metal; X=S,Se,Te) from the respective oxide nanoparticles, is a slow diffusion-controlled process, which is limited to reactive oxides such as WO_3 and therefore is not possible for less reactive oxides, such as those of titanium and niobium. To try and alleviate these deficiencies, a new strategy was developed whereby metal halides or carbonyls are used as precursors. These compounds have high vapour pressure at temperatures below 300 °C and are very unstable, reacting with H_2X (X=S,Se,Te) vapour instantaneously. This reaction leads to fast nucleation of incipient MX_2 nuclei, which grow outwards in a layer-by-layer fashion. Fullerene-like NbS_2 nanoparticles[21] were the first to be synthesized according to this strategy. Subsequently, TiS_2 nanotubes (ref. 22) and fullerene-like MoS_2 ($MoSe_2$) (ref. 23), WS_2 (ref. 24), and TiS_2 (ref. 25) nanoparticles were synthesized by the reaction of the respective metal halide with a sulphur reagent.

The synthesis of very uniform single-wall nanotubes of the multinary compound $SbPS_{4-x}Se_x$ was recently reported[26]. The sulphur-to-selenium exchange led to a red shift in the absorption coefficient of the nanotubes. Various metal oxide nanotubes were synthesized through soft chemistry ('chemie douce') processes, such as hydrothermal, sol-gel, intercalation–exfoliation, sonochemical reactions, and so on. V_2O_{5-x}-alkylamine nanotubes, which have been studied extensively in the past, were recently used as a template for the synthesis of VS_2 nanotubes[27]. This work is remarkable in so far as the bulk lamellar phase of VS_2 does not exist, which is another manifestation of the inherent stability of these nanotubular phases. Reversible electrochemical copper-ion intercalation in the VS_2-alkylamine nanotubes was also demonstrated in this work.

Recently, the first oxihalide nanotubes of the layered compound WO_2Cl_2 were prepared using a chemie-douce process[28]. Layered structures are also prevalent for hexavalent uranium oxo- compounds owing to the strong tendency of the U^{6+} ion to form linear uranyl ions, UO_2^{2+}. The synthesis of an ordered array of $[(UO_2)_3(SeO_4)5]^{4-}$ nanotubes in a room-temperature reaction in aqueous solution was recently reported[29].

A remarkable manifestation of the kinetic stabilization of closed fullerene-like nanostructures was demonstrated recently in the synthesis of fullerene-like nanoparticles from the layered compound Cs_2O (ref. 10). Films with a Cs/O ratio of approximately 2:1 are known to reduce the electron work function, increasing the sensitivity of optoelectronic detectors, used, for example, in medical imaging. Unfortunately, these films are highly reactive and are damaged by even a short exposure to low vacuum conditions. Nested closed nanoparticles

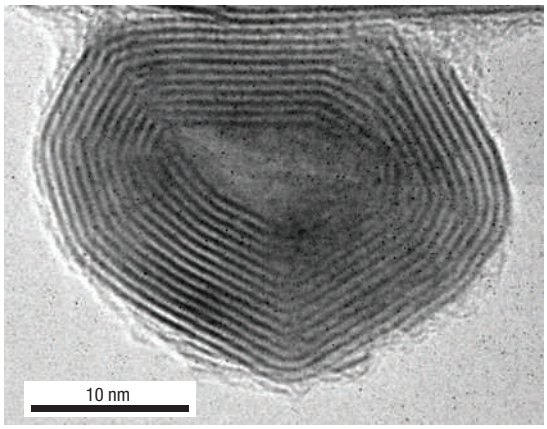

Figure 2 TEM image of a closed-cage (fullerene-like) nested Cs_2O nanostructure obtained by intense solar irradiation of pure crystalline Cs_2O powder in vacuum. The measured layer-to-layer distance is 0.635–0.645 nm (refs 10,11). Although the structure of the closed nanoparticle is not free of defects, its overall closed structure provides remarkable kinetic stabilization against reaction with oxygen, CO_2 and water in the ambient atmosphere. This behaviour is not unique to this particular kind of nanoparticle. It is also common to the fullerene-like nanoparticles and nanotubes of metal dihalides, such as $NiCl_2$ (ref. 9). Reproduced with permission from ref. 11. Copyright (2006) Wiley-VCH.

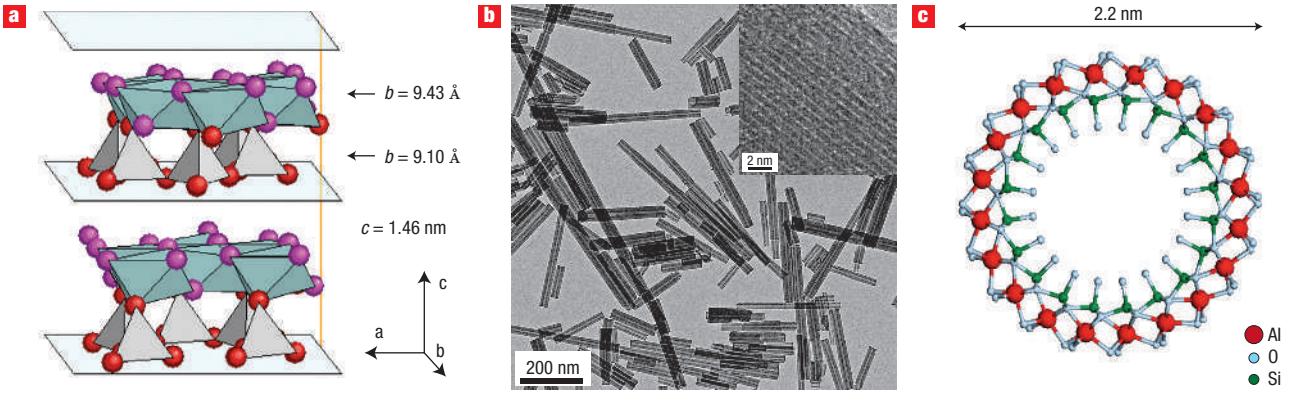

Figure 3 Naturally occurring nanotubes are made of lattices with built-in asymmetry and have been known for many years[1]. **a**, A schematic rendering of the lattice of chrysotile (magnesium hydroxide silicate). The length of each repeating unit along the *b* axis of the magnesium hydroxide octahedra (green) is longer than that of the silica tetrahedra (grey). Reprinted with permission from ref. 30. Copyright (2004) Wiley-VCH. **b**, A TEM micrograph of synthetic multiwall asbestos nanotubes (chrysotile). The inset shows an enlarged TEM image of the wall of an individual chrysotile nanotube with well-resolved magnesium hydroxide silicate molecular sheets 0.74 nm apart. (Nanotubes synthesized by N. Roveri.) **c**, A cross section of alumino-silicate (imogolite) nanotubes. Reprinted with permission from ref. 32. Copyright (2005) ACS. The structure of such nanotubes was first studied by Pauling[1] who suggested that the driving force for the formation of the nanotubes lies in the built-in asymmetry of the unit cell along the *b*-axis. Thus the larger octahedra (magnesium hydroxide in **a**, and alumina in **c**) are present on the outer perimeter of each layer in the nanotube and the smaller silica tetrahedra occupy the inner perimeter. In contrast to naturally occurring chrysotile nanotubes and fibres, the synthetic nanotubes were found to be non-toxic offering them numerous applications in future construction materials.

of Cs_2O were observed in laser-ablated powder, initially in tiny amounts and subsequently, using solar ablation, in larger quantities (Fig. 2). Remarkably though, these fullerene-like nanoparticles suffered only slow degradation in the ambient atmosphere.

Naturally occurring nanotubes of asbestos-related minerals, like chrysotile (magnesium hydroxide silicate) and kaolinite (alumino-silicate) have been known for many years and investigated in the past[1] (see Fig. 3a for a schematic drawing of the chrysotile lattice). The lattice mismatch between the magnesium hydroxide or alumina octahedra and the smaller silica tetrahedra leads to a strong built-in strain, and consequently, a bending force arises with the convex magnesium hydroxide or alumina octahedra appearing in the outer perimeter and the concave silica tetrahedra in the inner perimeter (Fig. 3c), thereby forming nanotubes (Fig. 3b). Incidentally, Pauling concluded that layered materials, such as MoS_2 and $CdCl_2$, having no asymmetric structure and therefore no built-in strain, are not likely to form closed structures like nanotubes, which is obviously not the case today. Stoichiometric nanotubes of chrysotile were obtained in large yields only quite recently[30,31]. Most astonishingly, whereas the biotoxicity of naturally occurring asbestos is well documented, synthetic chrysotile nanotubes were found to be completely benign[31], suggesting that in the future they could replace the banned natural asbestos fibres in construction materials. Also recently, single-wall alumino-germanate and silicate nanotubes with imogolite structure (see Fig. 3c) were obtained by a soft-chemistry process[32].

Nanotubes of the graphite-like boron nitride compound were among the first to be studied. Using metal oxides as catalysts, the large-scale synthesis of multiwall BN nanotubes was recently reported[33]. Further purification of the nanotubes was obtained through polymer wrapping of the nanotube backbone and secretion of obstinate boron nitride residues[34].

Crystalline nanotubes (or hollow nanofibres) of quasi-isotropic three-dimensional compounds were recently obtained, for example, by depositing a precursor on a one-dimensional template such as porous anodized aluminium oxide (AAO), and soft templates, such as elongated micelles. Similarly, faceted GaN nanotubes with hexagonal cross-sections were produced by the reaction of trimethylgallium and ammonia on a template of an ordered array of ZnO nanowires, which was subsequently removed[12]. Carbothermal synthesis was used ingeniously to synthesize nanotubes of various three-dimensional oxides, nitrides and sulphides[13,14]. In one such example the heated graphite crucible also served to reduce the solid precursor M_2O_3 (M=Al,Ga,In) producing a volatile intermediate, M_2O, which subsequently reacted with nitrogen (or ammonia) producing MN nanotubes with faceted cross-sections. Recently, a new synthetic strategy was promoted, whereby nanorod precursors are first synthesized. These nanorod templates are converted into nanotubes through self-sacrificial chemistry. Two examples of this approach are the synthesis of spinel ($ZnAl_2O_4$) (ref. 35), and Zn_3P_2 and Cd_3P_2 nanotubes (ref. 36).

Numerous reports on the use of AAO membrane as a template for the growth of various nanotubes and nanowires have appeared in recent years. Nanotubes with walls made of gold nanoparticles instead of gold atoms only were obtained by chemical deposition of the gold nanoparticles into a silanized AAO membrane[37]. Nanotubes made of self-assembled SnO_2 nanoparticles were prepared using a similar method[38], and were used as the host material for Li intercalation batteries. Crystalline Fe_3O_4 nanotubes, which exhibited small magnetoresistance behaviour at 77 K, have also been reported[39].

THEORETICAL CALCULATIONS

With the advent of first-principle computational methods, analysis of inorganic nanotubes and fullerene-like structures became possible, bringing new insight and predicting new properties, some of them yet to be verified by experiment. The structure, energetics and the electronic structure of double-wall BN nanotubes were recently discussed[40]. The most stable double-wall tubes are those with minimum overlap between adjacent boron and nitrogen atoms of the two concentric tubes, which is fulfilled by zig-zag nanotubes. Some overlap is inevitable in armchair nanotubes, making them less stable than zig-zag nanotubes.

Numerous nanotubes with graphite-like ('sp^2'-like or sheet-like) lattice and cylindrical shape were studied using density functional

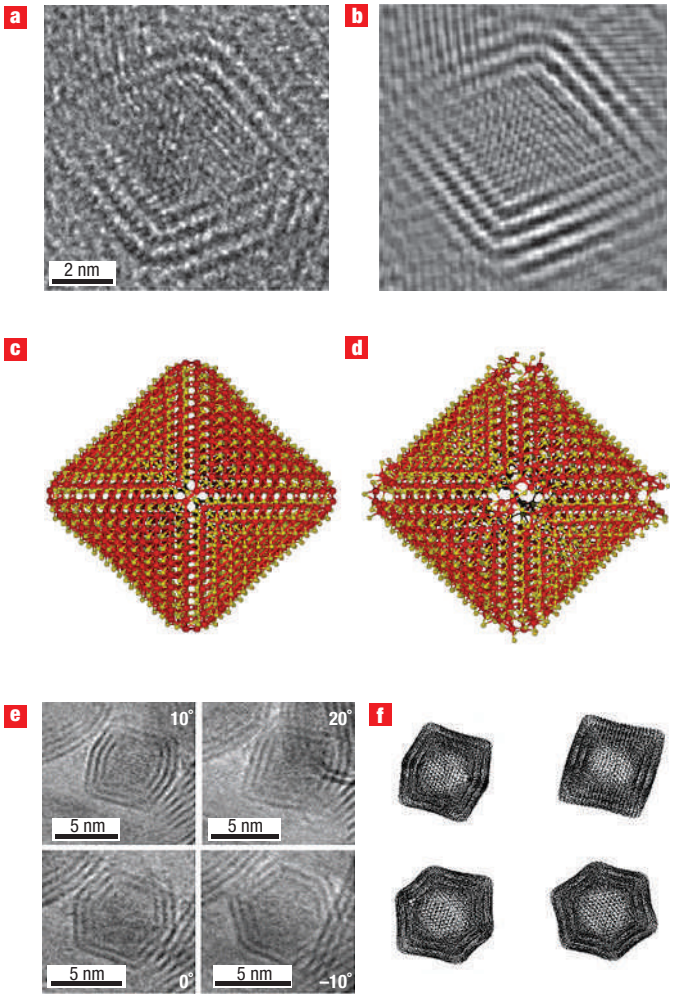

Figure 4 Hollow nano-octahedra, 3–6 nm in size and 2–5 layers thick were found in laser-ablated samples of different layered compounds, such as MoS_2, $NiCl_2$, SnS_2. They were generally found to have a chemical composition almost identical to the bulk material, somewhat analogous to C_{60} in the carbon fullerene series. They are believed to have a rhombus in each of their six corners. A typical high-resolution TEM micrograph of an octahedral MoS_2 nanoparticle (**a**) and its filtered Fourier transform image (**b**). The distance between each MoS_2 layer is 0.61 nm. A $Mo_{576}S_{1140}$ octahedron calculated from first principles using a density-functional tight-binding (DFTB) algorithm at 0 K (**c**) and after molecular dynamic (MD) simulation at 300 K (**d**). The starting model was $(MoS_2)_{576}$ (corner to corner distance of 3.8 nm), which relaxed by losing two sulphur atoms per corner (12 in total). **e**, A TEM image of a three-layered nano-octahedron at various tilt angles. **f**, The corresponding images of the semi-empirically calculated atomic model for a $(MoS_2)_{784}@(MoS_2)_{1296}@(MoS_2)_{1936}$ octahedral fullerene. Note the visual similarity between the experimentally observed nano-octahedron (**e**) and the calculated structure (**f**). According to the DFTB–MD calculations, the MoS_2 nano-octahedra were found to be metallic, but this remains to be confirmed by experiment. Reprinted with permission from ref. 43. Copyright (2006) Wiley-VCH.

theory methodology[41]. Many of the studied nanotubes are known to possess a zincblende or wurtzite ('sp^3'-like or diamond-like) lattice with tetrahedral arrangement of the atoms in the bulk. Their graphitic phase is either unknown or unstable. For example, the graphitic AlN nanotubes are higher in energy by as much as 0.68 eV per atom compared with bulk zincblende (diamond-like) AlN. Experimentally synthesized nanotubes from group III and group V elements, such as AlN or GaP, have a zincblende (or wurzite) structure and are highly faceted. Therefore, the relevance of the computational effort to the experimental investigation of such nanotubes is not clear at this point.

$MgCl_2$ is a compound with layered $CdCl_2$ structure, in which the Mg atoms form a sheet sandwiched between two atomic sheets of chlorine. In analogy to the MoS_2 structure, the coordination numbers of the Mg and Cl are six and three, respectively. The structure of $MgCl_2$ nanotubes was elucidated recently by quantum chemical calculations[42]. Although nanotubes with different coordination numbers were also attempted, those with the layered $CdCl_2$ structure were found to be the most stable for diameters of 2.5 nm and above. Experimentally, nanotubes and fullerene-like structures of various metal halides have been synthesized in the past[9,19].

Early on it was recognized that rhombi rather than pentagonal rings, which occur in carbon fullerenes and nanotubes, are the favourable elements in polyhedra of layered compounds[7]. Fig. 4a, b shows a MoS_2 nano-octahedron consisting of four layers, each with rhombi in their six corners. Multiwall nano-octahedra, with the inner wall being made up of about 600–800 molybdenum and 1,200–1,600 sulphur atoms, respectively, are routinely found in laser-ablated samples of various compounds with layered structure[43,44], nonetheless in minute quantities.

Very recently, detailed density-functional tight-binding coupled with molecular dynamics (DFTB–MD) theoretical analysis for MoS_2 nano-octahedra was undertaken, permitting a direct comparison with experimental data[43]. Figure 4c shows a stable $Mo_{576}S_{1140}$ octahedron obtained by DFTB calculations at 0 K (left). After MD simulation to 300 K (right) the edges and corners become distorted, but the overall structure of the nano-octahedron is preserved. Furthermore, using a few other simplifications, the calculations could be extended to any size, and the phase stability could be compared with that of MoS_2 nanoparticles with different structures. Figure 4e, f compares TEM and computer generated images of MoS_2 nano-octahedra under various tilt angles. The great similarity between the experimental and calculated images is compelling and gives further credibility to that analysis. Figure 5 shows the energy diagram of the various species as a function of their size. A few important conclusions can be drawn from this combined theoretical–experimental study: (1) the nano-octahedra are stable over a limited range of about 5,000–100,000 atoms (3–6 nm). Below this size, MoS_2 nanoplatelets are more stable, whereas quasi-spherical closed-cage (fullerene-like) nanoparticles become the most stable species above the higher limit. At even larger sizes (approximately 10^7 atoms) macroscopic MoS_2 platelets become the most stable structure. (2) Among the possible stable nano-octahedra structures those with the formula Mo_nS_{2n-12} seem to be the most stable. (3) Whereas MoS_2 platelets and the quasi-spherical nested structures are semiconductors, the nano-octahedra are metallic. Despite there being only small overall chemical differences between structures, the nano-octahedra seem to be the most stable in the size range of a few nm. The structures do however have completely different physical properties.

PHYSICAL PROPERTIES

The physical characteristics of macroscopic structures, be it mechanical, optical or electronic properties, are influenced by the intrinsic properties of the material as well as by various extrinsic factors, such as impurities, defects, deviations from stoichiometry and so on. In contrast, nanostructured moieties can be made (almost) perfectly crystalline, and therefore their behaviour is exclusively determined by the intrinsic structure and the chemical bonding, rendering quantitative comparison with first-principle

calculations possible. The physical and chemical properties of inorganic nanotubes are variable and largely depend on the property of the bulk compound from which they are derived. Thus, BN (ref. 40), MoS_2 (ref. 43) and $NbSe_2$ (ref. 45) nanotubes are, insulators, semiconductors and superconductors, respectively.

ELECTRONIC STRUCTURE

Whereas quantum dots exhibit a blue shift with decreasing size of the nanoparticle, both experiment and theory has shown in the past that the bandgap of semiconducting nanotubes, such as GaSe and MoS_2, shrinks with decreasing nanotube diameter. This effect can be ascribed to two factors: (1) small quantum size effect of the closed nanostructures, and (2) the deformation of the chemical bonds in the curved sheet leading to a less than perfect hybridization of the atomic orbitals. Furthermore, whereas armchair nanotubes were often found to have an indirect (Δ–Γ) electronic transition, zig-zag nanotubes possess a direct (Γ–Γ) transition suggesting that they could emit strong luminescence on optical or electrical excitation[9]. Numerous publications have been dedicated to the calculations of the band structure of nanotubes, such as AlN (ref. 41) and SiC (ref. 46) with an 'sp^2'-like (graphitic) lattice, which differs from the bulk material characterized by an 'sp^3'-diamond-like (zincblende or wurzite) structure. Generally, their calculated properties resemble those of nanotubes from genuine layered compounds. BN nanotubes were found to have a high bandgap irrespective of their chirality. Both experiment and theory show that the bandgap of such nanotubes shrinks to the point where they become metallic (giant Stark effect) with the application of a large transversal electric field[47,48].

MECHANICAL PROPERTIES

Tensile and buckling tests were performed on individual WS_2 nanotubes with a scanning electron microscope (SEM)[49]. Figure 6 displays a WS_2 nanotube compressed against the surface of a Si wafer. The Young's modulus of the nanotube was found to be 150 GPa, that is, about one-seventh of the value of carbon nanotubes. Independent tensile tests showed that the nanotubes behave elastically almost up to their failure. The Young's modulus, yield strength and elongation to failure are 150 GPa, 16 GPa and 12%, respectively[49]. *Ab initio* calculations were on the high side but nevertheless in good agreement with the experimental data. The experimentally determined yield strength/Young's modulus ratio of 0.11 is an exceedingly high value in comparison with other high-strength materials. These observations indicate that the failure of the nanotubes is initiated by the rupture of an individual chemical bond, and that the role of macroscopic mechanisms, such as presence of dislocations, dislocations-migration and propagation of cracks along grain boundaries, are completely irrelevant here. It is also notable that the measured values of the yield strength of carbon nanotubes (20–250 GPa) (ref. 50) suffer from large scattering, probably owing to structural imperfections in their structure.

APPLICATIONS

MECHANICAL, INCLUDING TRIBOLOGICAL APPLICATIONS

The quasi-spherical shape of the fullerene-like WS_2 and MoS_2 nanoparticles and their inert sulphur-terminated surface suggested that they could serve as superior solid lubricants in the form of additives to lubrication fluids, greases and for self-lubricating coatings[15]. These advances led to a surge of interest in this technology from a very large variety of industries, having virtually no common denominator other

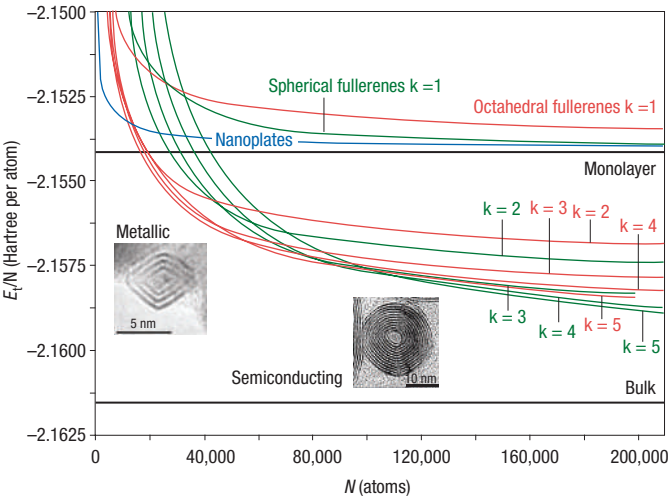

Figure 5 The energies per atom E_t/N of various MoS_2 nanostructures is presented as a function of its size (N is the total number of atoms). The calculations were carried out by a semi-empirical model[43]. The different calculated nanostructures are: multilayered octahedral fullerenes (red) and fullerene-like spherical nanoparticles (green), with different numbers of MoS_2 walls, k; triangular nanoplatelets (blue) are also calculated. Note that, according to calculations, the multiwall nano-octahedra are the most stable moieties from about 5,000–100,000 atoms (3–6 nm). This range extends to higher values than those obtained experimentally (the largest nano-octahedra observed in the experiments contained 25,000 Mo and S atoms). This discrepancy can be attributed to the approximations made in the model. Note also that the nano-octahedra are metallic according to the DFTB–MD calculations, whereas all the other forms of MoS_2 are semiconductors. This important fact is yet to be confirmed experimentally. Reprinted with permission from ref. 43. Copyright (2006) Wiley-VCH.

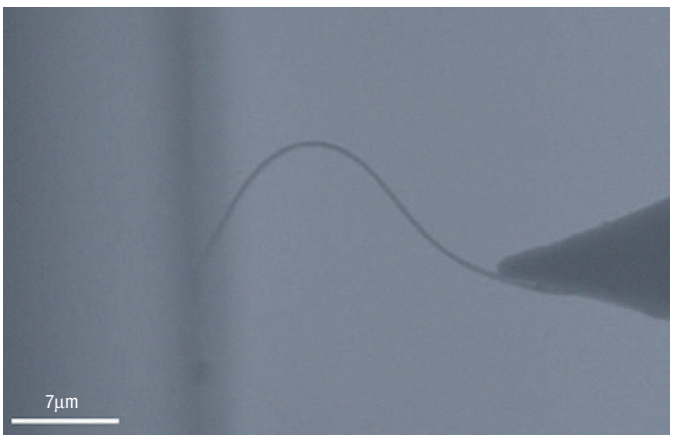

Figure 6 Tensile strength, bending and compression experiments on individual WS_2 nanotubes were carried out, providing quantitative data on the mechanical properties of these nanostructures. Shown here is an SEM image in which a WS_2 nanotube is compressed against the surface of a silicon wafer. The nanotube was glued to a cantilever by electron-beam irradiation in the presence of carbon vapours, which can easily be afforded in the SEM. It was pushed against a mirror flat silicon wafer surface using a micromanipulator. Note the flexibility of the elastic nanotube. Using known elastic models, the Young's modulus of the nanotubes was determined to be 150 GPa, that is, about one-seventh of the value of a carbon nanotube. Reprinted with permission from ref. 48. Copyright (2005) National Academy of Sciences, USA.

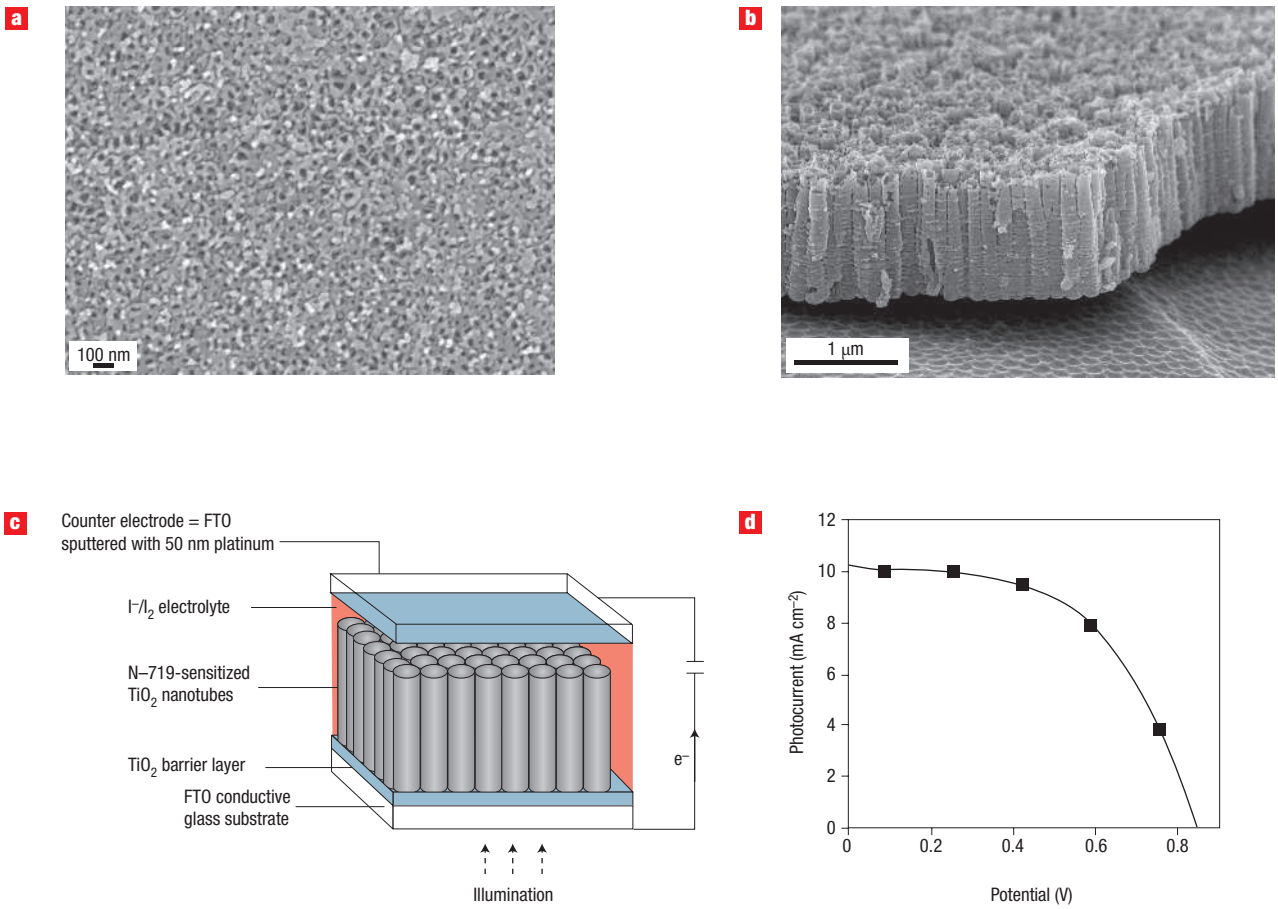

Figure 7 Anodization of titanium film, deposited on a conductive glass in acidic solutions containing HF, leads to the formation of a dense array of interconnected polycrystalline titania (TiO_2) nanotubes. This film can then be integrated into a dye-sensitized solar cell. **a**, An edge-on SEM image of a film made of an array of titanium nanotubes (46 nm in diameter and 17 nm wall thickness). Titanium film (4 μm) was deposited on fluorine-doped tin oxide film on glass and anodized at 12 V in 0.5% HF–acetic acid electrolyte. The film was immersed in 0.2 M $TiCl_4$ solution for 1 h and subsequently annealed for 3 h in air at 450 °C. **b**, The same film viewed by SEM, side-on. **c**, Schematics of a front-side-illuminated dye-sensitized solar cell. The film was soaked in Ru-bipyridine-based dye (N-719, Solaronix). The electrolyte contained 0.5 M LiI, 0.05 M I_2, 0.6 M *N*-methylbenzimidazole, 0.10 M guanidinium thiocyanate and 0.5 M tert-butylpyridine in methoxypropionitrile. A fluorine-doped tin oxide (FTO) conductive glass slide sputter-coated with 25 nm of Pt was used at the counter electrode. **d**, A current–voltage (*I–V*) curve under AM1.5 solar simulator illumination (100 mW cm^{-2}). The power output of this cell is given by *I* x *V* (8 x 0.59 = 4.7 mW) at the point of maximum power. The efficiency is power output/power input x 100 = 4.7%. The high photocurrent can be attributed to the large surface area of the nanotubes, the vectorial charge transport along the walls of the nanotube and the reduced electron–hole recombination of the anodized surface. This architecture minimizes losses occurring in nanoparticle-based photoelectrodes owing to the hopping of charge carriers across nanoparticle boundaries. Reprinted with permission from ref. 65. Copyright (2006) IOP.

than the need to reduce friction and wear. Numerous development programmes are underway, some of them at a very advanced stage or even having made products. The first medical application — alleviating friction in orthodontic wires — was recently demonstrated[51], with numerous others to follow. Toxicological tests on the fullerene-like WS_2 nanoparticles concluded that they are safe[52]. Mechanistic studies indicate that the spherical MS_2 nanoparticles exhibit rolling (sliding) friction under mild loads (<0.5 GPa) (hydrodynamic lubrication). Under heavier loads, where the spacing between the mating surfaces is small (mixed and boundary lubrication conditions), the nanoparticles slowly deform and exfoliate giving up WS_2 layers that stick to the underlying surfaces and provide easy shear[15,53].

In another series of experiments, fullerene-like WS_2 and MoS_2 nanoparticles were shown to withstand shockwaves of up to 25 and 30 GPa, respectively, with concurrent temperatures rising up to 1,000 °C (ref. 54). No evidence for significant structural degradation or phase changes was observed, making these materials probably the strongest cage molecules known today and offering them a plethora of applications for shielding; in cars and, in the future, perhaps also as additives to strengthen construction materials. Furthermore, Raman measurements of these nanoparticles indicated no degradation under hydrostatic pressures of 20 GPa, indicating again their high-pressure resilience[55]. It is noticeable that carbon nanotubes and fullerenes are unlikely to be stable under high pressure owing to the 1.7 GPa graphite-to-diamond transformation[56].

SENSING APPLICATIONS, ELECTRONICS AND QUANTUM HARVESTING

Room-temperature ferromagnetic VO_x-alkylamine nanotubes, which could be useful for spintronics, were obtained by lithium and iodine intercalation[57]. Moreover, the doping has the effect of shifting the Fermi level from the middle of the energy gap to either

the valence (iodine) or the conduction band (lithium), turning this Mott-Hubbard insulator into a good conductor.

A number of interesting observations were recently made with titanate nanotubes of the formula $H_2Ti_3O_7$. By adding these nanotubes to organic light-emitting diodes, the luminosity was improved and the turn-on voltage decreased. These effects were attributed to the lower barrier for hole injection from the electrode to the organic semiconductor and to the improved hole transport in the organic film[58]. In another recent study, enhanced electrochromism was observed in films made of titanate nanotubes[59]. The titanate nanotube films were shown to exhibit faster proton diffusion and higher capacity than those made of TiO_2 (anatase) nanoparticles. Intercalating iron atoms in titanate nanotubes was shown to lead to a significant red shift of the absorption edge, and to interesting magnetic characteristics[60].

A biosensor for dopamine, which is an important marker for neurodegenerative diseases such as Parkinson's disease, based on titanate nanotube films deposited on glassy carbon electrodes, was recently reported[61]. Electrochemical measurements showed that the reduction peak of the dopamine was well separated from that of ascorbic and uric acids, which is not easily achievable in physiological solutions. This observation was attributed to the negative charge of the nanotube, attracting the positively charged dopamine moieties and excluding the negatively charged ascorbic and uric acid ions. In another series of remarkable studies, arrays of polycrystalline titania nanotubes were prepared by electrochemical anodization of titanium foil[62]. The nanotube array was coated with a 10 nm palladium film and its resistivity as a function of H_2 concentration in the gas atmosphere was monitored, showing perhaps the highest hydrogen sensitivity for any known hydrogen sensor, suggesting various possible medical and environmental applications. Optimizing the Ti anodization process, the authors have developed a water photocleavage system, which showed 7.9% photoconversion efficiency in the 320–400 nm range[63]. A dye-sensitized photoelectrochemical cell based on the titania nanotube films with overall 4.7% conversion efficiency was also reported (Fig. 7)[64,65]. The large surface area of the nanotube array, coupled with its low electron-hole recombination and efficient vectorial charge transport along the nanotube axis were among the reasons for the reported high efficiencies of the cell.

Nanofluidic devices based on polycrystalline metallic and metal oxide nanotubules have been used in the past for biomolecule diagnostics[66]. More recently, perfectly crystalline and very narrow (<20 nm) nanotubes were used as a platform for nanofluidics and unipolar charge transport[67]. The synthesized silica nanotubes were integrated in a metal oxide (KCl) solution field-effect transistor (MOSolFET) (Fig. 8). The conductance of the potassium ion (majority carrier) within the p-type nanotube channel was modulated by controlling the gate voltage. Furthermore, the translocation of individual DNA molecules in sub-femtolitre concentrations through the nanotube channel could be detected as a temporary current drop or rise.

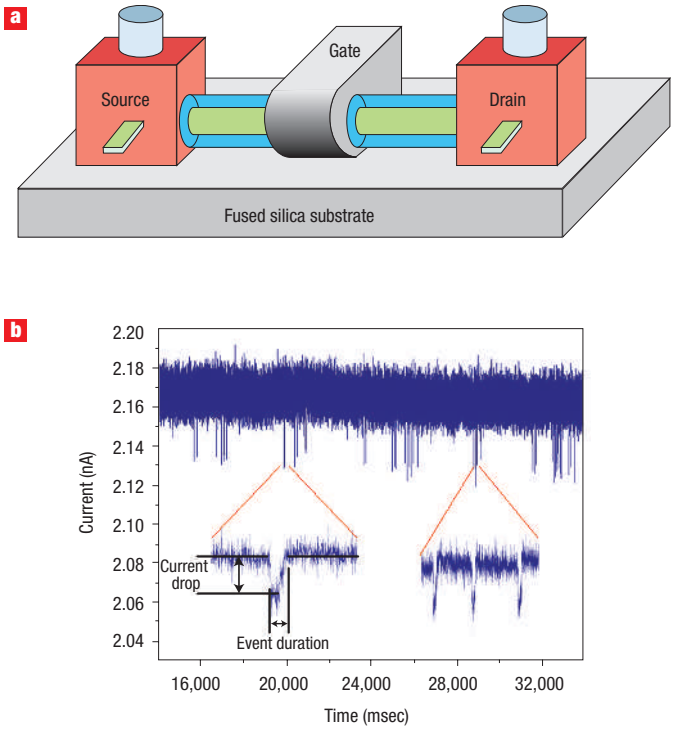

Figure 8 A single nanotube metal-oxide solution field effect transistor (MOSolFET) could be considered as the ionic analogue of the electronic field-effect transistor. The diameter of the nanotube (nanochannel) where the fluid flows is smaller than twice the thickness of the electrical double layer (Debye length) of the electrolyte solution. Therefore, there is no charge balance in the centre of the nanotube and if the surface of the nanotube is made negative by the gate electrode, the flowing solution becomes more concentrated with respect to the cations inside the nanotube channel. **a**, Schematics of the MOSolFET device with a silica nanotube (blue), which can serve as a detector for a single DNA molecule. **b**, The temporary drops in the current–time trace are markers for a single DNA molecule passage through the nanotube. Measurements were carried out in 2 M KCl solution. Reprinted with permission from ref. 67. Copyright (2006) ACS.

CATALYSIS AND BIOTECHNOLOGY

In a very elegant study, hollow nanoparticles of MoS_2, albeit with non-perfect crystallinity, were prepared by sonochemical reactions of $Mo(CO)_6$ in the presence of silica nanoparticles, which served as a template and were subsequently removed by HF etching and annealing[68]. These nanoparticles revealed high reactivity and selectivity towards hydrodesulphurization of thiophene. In a more recent study, Ni nanoparticles were deposited onto a MoS_2-nanotube support. A very reactive and selective catalyst for hydrodesulphurization of thiophene and a few of its derivatives was obtained[69]. These kinds of catalysts could play a major role in mitigating the environmental impact of sulphur-rich gasoline. Also recently, $(BiO)_2CO_3$ nanotubes were shown to exhibit a very strong antibacterial reactivity for *Helicobacter pylori*, which is implicated in peptic ulcers and gastritis[70]. Immobilization of various proteins and biomolecules, such as ferritine, cytochrome-c, strepavidin and glucose oxide onto multiwall BN nanotubes was demonstrated[71], suggesting numerous biotechnological and medical applications for such nanostructures. Various nanotubes, such as those of titanate or VO_x-alkylamine, which are produced by chemie-douce processes, are in fact nanoscrolls, which can be unwrapped, by varying the pH, for example. This attribute offers the possibility to use them as drug carriers for targeting specific tissues or tumours.

ELECTROCHEMICAL APPLICATIONS

A solution-based lithium intercalation of TiS_2 nanotubes with the formal charge of one lithium atom/TiS_2 molecule makes up one of many studies on nanotube-based intercalation batteries[22]. The same group also showed that high-purity TiS_2 nanotubes with open-ended tips can efficiently store 2.5 wt% of hydrogen at 298 K under pressure of 4 MPa (ref. 72). Detailed analysis showed that about 1 wt% of the hydrogen is chemisorbed and the rest of the hydrogen atoms are physisorbed to the nanotubes. Relatively

large amounts of lithium could be inserted into $MoS_2I_{0.3}$ nanotube bundles (up to 3 mol Li per mol MoS_2), which were prepared by chemical vapour transport[73]. Comparing their electrochemical behaviour with those of bulk 2H-MoS_2, one finds a significant increase in the amount of inserted lithium and a decrease of about 0.7 V in the onset potential for lithium insertion for the nanotube electrodes. The electron spin resonance signal of lithiated $MoS_2I_{0.3}$ nanotube bundles decreased upon air exposure, but at a much slower rate than lithiated bulk 2H-MoS_2 crystals, indicating the greater stability of the lithiated nanotubes compared with lithiated bulk MoS_2.

A number of Li intercalation studies of VO_x-alkylamine nanotubes were reported in the past. Li intercalation was also studied in titanate[74] and SnO_2 (ref. 38) nanotubes. The energy density of the titanate nanotube-based electrode was 210 mA h g^{-1} at a current density of 0.24 A g^{-1}. The capacity remained high even at relatively high discharge rates (144 mA h g^{-1} at a current density of 3.6 A g^{-1}, respectively). Furthermore, the electrode was found to be stable during many charge/discharge cycles. The capacity of the SnO_2 nanotube-based electrode was reported to be 525 mA h g^{-1} after 80 cycles[38]. Polycrystalline $Ni(OH)_2$ tubes coated with 5 wt% $Ca(OH)_2$, $Co(OH)_2$, or $Y(OH)_3$ were prepared using an AAO template[75]. The electrochemical measurements showed that both pure and coated $Ni(OH)_2$ tube electrodes exhibited electrochemical performance superior to that of a conventional electrode made of spherical $Ni(OH)_2$ particles. The pure $Ni(OH)_2$ tube electrode displayed the highest discharge capacity of 315 mA h g^{-1}, but the $Co(OH)_2$-coated electrode exhibited higher recycling stability.

CONCLUSIONS

Inorganic nanotubes and fullerene-like nanostructures are a generic structure of inorganic layered two-dimensional compounds. In some cases, such as WS_2, MoS_2, BN and V_2O_5, fullerene-like nanoparticles and nanotubes are produced in gross amounts. However, size and shape control is still in its infancy. More recently, nanotubes of numerous inorganic compounds with non-layered structure have been prepared using various templates. Study of these novel nanostructures has led to the observation of a number of interesting properties offering numerous potential applications in tribology, high-energy-density batteries, sensors, photoconversion of solar energy and nanoelectronics.

doi:10.1038/nnano.2006.62

References

1. Pauling, L. The structure of the chlorites. *Proc. Nat. Acad. Sci. USA* **16,** 578–582 (1930).
2. Bicerano, J. Maryanick, D. S. & Lipscomb, W. N. Molecular orbital studies on large closo boron hydrides. *Inorg. Chem.* **17,** 3443–3453 (1978).
3. Lipscomb, W. N. and Massa, L. Examples of large closo boron hydride analogs of carbon fullerenes. *Inorg. Chem.* **31,** 2297–2299 (1992).
4. Kroto, H. W., Heath, J. R., O'Brien, S. C., Curl, R. F. & Smalley, R. E. C_{60}: Buckminsterfullerene. *Nature* **318,** 162–163 (1985).
5. Iijima, S. Helical microtubules of graphitic carbon. *Nature* **354,** 56–58 (1991).
6. Tenne, R., Margulis, L., Genut M. & Hodes, G. Polyhedral and cylindrical structures of tungsten disulphide. *Nature* **360,** 444–445 (1992).
7. Margulis, L., Salitra, G., Tenne, R. & Talianker, M. Nested fullerene-like structures. *Nature* **365,** 113–114 (1993).
8. Feldman, Y., Wasserman, E., Srolovitz D. J. & Tenne R. High rate gas phase growth of MoS_2 nested inorganic fullerene-like and nanotubes. *Science* **267,** 222–225 (1995).
9. Rosenfeld Hacohen Y. *et al.* Synthesis of $NiCl_2$ nanotubes and fullerene-like structures by laser ablation. *Phys. Chem. Chem. Phys.* **5,** 1644–1651 (2003).
10. Albu-Yaron A. *et al.* Preparation and structural characterization of stable Cs_2O closed-cage structures. *Angew. Chem. Int. Edn* **44,** 4169–4172 (2005).
11. Albu-Yaron, A. *et al.* Synthesis of fullerene-like Cs_2O nanoparticles by concentrated sunlight, *Adv. Mater.* (in the press).
12. Goldberger, J. *et al.* Single-crystal gallium nitride nanotubes. *Nature* **422,** 599–602 (2003).
13. Li, Y., Bando, Y. & Golberg, D. Single-crystalline In_2O_3 nanotubes filled with In. *Adv. Mater.* **15,** 581–585 (2003).
14. Yin, L. W., Bando, Y., Golberg, D. & Li, M. Growth of single-crystal indium nitride nanotubes and nanowires by controlled carbon-nitridation reaction. *Adv. Mater.* **16,** 1833–1838 (2004).
15. Rapoport, L., Fleischer. N. & Tenne, R. Applications of WS_2 (MoS_2) inorganic nanotubes and fullerene-like nanoparticles for solid lubrication and for structural nanocomposites. *J. Mater. Chem.* **15,** 1782–1788 (2005).
16. Tenne, R. & Rao, C. N. R. Inorganic nanotubes. *Phil. Trans. R. Soc. Lond. A* **362,** 2099–2125 (2004).
17. Remskar, M. Inorganic nanotubes. *Adv. Mater.* **16,** 1497–1504 (2004).
18. Patzke, G. R., Krumeich, F. & Nesper, R. Oxidic nanotubes and nanorods–anisotropic modules for a future nanotechnology. *Angew. Chem. Int. Edn* **41,** 2446–2461 (2002).
19. Tenne, R. Advances in the synthesis of inorganic nanotubes and fullerene-like nanoparticles. *Angew. Chem. Int. Edn* **42,** 5124–5132 (2003).
20. Rao, C. N. R. & Nath, M. Inorganic nanotubes. *Dalton Trans.* 1–25 (2003).
21. Schuffenhauer, C., Popovitz-Biro, R. & Tenne, R., Synthesis of NbS_2 nanoparticles with (nested) fullerene-like structure (*IF*). *J. Mater. Chem.* **12,** 1587–1591 (2002).
22. Chen, J., Tao, Z. L. & Li, S. L. Lithium intercalation in open-ended TiS_2 nanotubes. *Angew. Chem. Int. Edn* **42,** 2147–2151 (2003).
23. Etzkorn, J. *et al.* Metal-organic chemical vapor deposition synthesis of hollow inorganic-fullerene-type MoS_2 and $MoSe_2$ nanoparticles. *Adv. Mater.* **17,** 2372–2375 (2005).
24. Li, X. P., Ge, J. P. & Li, Y. D. Atmospheric pressure chemical vapor deposition: An alternative route to large-scale MoS_2 and WS_2 inorganic fullerene-like nanostructures and nanoflowers. *Chem. Eur. J.* **10,** 6163 – 6171 (2004).
25. Margolin, A., Popovitz-Biro, R., Albu-Yaron, A., Rapoport, L. & Tenne, R. Inorganic fullerene-like nanoparticles of TiS_2. *Chem. Phys. Lett.* **411,** 162–166 (2005).
26. Malliakas, C. D. & Kanatzidis, M. G. Inorganic single wall nanotubes of $SbPS_{4-x}Se_x$ ($0 < x < 3$) with tunable band gap *J. Am. Chem. Soc.* **128,** 6538–6539 (2006).
27. Therese, H. A. *et al.* VS_2 nanotubes containing organic-amine templates from the NT-VO*x* precursors and reversible copper intercalation in NT-VS_2. *Angew. Chem. Int. Edn* **44,**262–265 (2005).
28. Armstrong, A. R., Canales, J. & Bruce, P. G. WO_2Cl_2 Nanotubes and nanowires. *Angew. Chem. Int. Edn* **43,** 4899–4902 (2004).
29. Krivovichev, S. V. *et al.* Nanoscale tubules in uranyl selenates. *Angew. Chem. Int. Edn* **44,** 1134–1136 (2005).
30. Falini, G. *et al.* Tubular-shaped stoichiometric chrysotile nanocrystals. *Chem. Eur. J.* **10,** 3043–3049 (2004).
31. Roveri, N. Geoinspired Synthetic Chrysotile Nanotubes. *J. Mater. Res.* (in the press).
32. Mukherjee, S., Bartlow, V. M. & Nair, S. Phenomenology of the growth of single-walled aluminosilicate and aluminogermanate nanotubes of precise dimensions. *Chem. Mater.* **17,** 4900–4909 (2005).
33. Zhi, C.Y., Bando Y., Tan C.C., Goldberg, D. Effective precursor for high yield synthesis of pure BN nanotubes. *Solid State Commun.* **135,** 67–70 (2005).
34. Zhi, C.Y. *et al.* Purification of boron nitride nanotubes through polymer wrapping. *J. Phys. Chem. B* **110,** 1525–1528 (2006).
35. Fan, H. J. *et al.* Monocrystalline spinel nanotube fabrication based on the Kirkendall effect. *Nature Mater.* **5,** 627–631 (2006).
36. Shen, G. *et al.* Single-crystalline nanotubes of II_3-V_2 semiconductors (submitted).
37. Sehayek, T., Lahav, M., Popovitz-Biro, R., Vaskevich, A. & Rubinstein, I. Template synthesis of nanotubes by room-temperature coalescence of metal nanoparticles. *Chem. Mater.* **17,** 3743–3748 (2005).
38. Wang, Y., Lee, J. Y. & Zeng, H. C. Polycrystalline SnO_2 nanotubes prepared via infiltration casting of nanocrystallites and their electrochemical application. *Chem. Mater.* **17,** 3899–3903 (2005).
39. Liu, Z. *et al.* Single Crystalline Magnetite Nanotubes. *J. Am. Chem. Soc.* **127,** 6–7 (2005).
40. Jhi, S.-H., Roundya, D. J., Louie, S. G. & Cohen, M. L. Formation and electronic properties of double-walled boron nitride nanotubes. *Solid State Comm.* **134,** 397–402 (2005).
41. Zhao, M., Xia, Y., Zhang, D. & Mei, L. Stability and electronic structure of AlN nanotubes. *Phys. Rev. B* **68,** 235415 (2003).
42. Linnolahti, M. & Pakkanen, T. A. Quantum chemical treatment of large nanotubes via use of line group symmetry: Structural preferences of magnesium dichloride nanotubes. *J. Phys. Chem. B* **110,** 4675–4678 (2006).
43. Enyashin, A. N. *et al.* Structure and stability of molybdenum sulfide fullerenes. *Angew. Chem. Int. Edn* (in the press).
44. Parilla, P. A. *et al.* Formation of nanooctahedra in molybdenum disulfide and molybdenum diselenide using pulsed laser vaporization. *J. Phys. Chem. B* **108,** 6197–6207 (2004).
45. Nath, M., Kar S., Raychaudhuri, A. K. & Rao, C. N. R. Superconducting $NbSe_2$ nanostructures. *Chem. Phys. Lett.* **368,** 690–695 (2003).
46. Zhao, M., Xia, Y., Li, F., Zhang, R. Q. & Lee, S. T. Strain energy and electronic structures of silicon carbide nanotubes: Density functional calculations. *Phys. Rev. B* **71,** 085312 (2005).
47. Khoo, K. H., Mazzoni, M. S. C. & Louie, S. G. Tuning the electronic properties of boron nitride nanotubes with transverse electric fields: A giant dc Stark effect. *Phys. Rev. B* **69,** 201401(R) (2004).
48. Ishigami, M., Sau, J. D., Aloni, S., Cohen, M. L. & Zettl A. Observation of the giant stark effect in boron-nitride nanotubes. *Phys. Rev. Lett.* **94,** 056804 (2005).
49. Kaplan-Ashiri, I. *et al.* On the mechanical behaviour of WS_2 nanotubes under axial tension and compression. *Proc. Natl. Acad. Sci. USA* **103,** 523–528 (2006).
50. Barber, A. H., Kaplan-Ashiri, I., Cohen, S. R., Tenne, R. & Wagner, H. D. Stochastic strength of nanotubes: An appraisal of available data. *Comp. Sci. Technol.* **65,** 2380–2384 (2005).
51. Katz, A., Redlich, M., Rapoport, L., Wagner, H. D. & Tenne, R. Improved orthodontic wires using fullerene-like WS_2 self-lubricating coatings. *Tribol. Lett.* **21,** 135–139 (2006).
52. Moore, G. E. Acute inhalation toxicity study in rats – limit test. Product safety laboratories, study number 18503. Dayton, New Jersey, USA 2006, Jan 18.
53. Joly-Pottuz, L. *et al.* Ultralow-friction and wear properties of *IF*-WS_2 under boundary lubrication. *Tribol. Lett.* **18,** 477–485 (2005).
54. Zhu, Y. Q. *et al.* Shock-absorbing and failure mechanism of WS_2 and MoS_2 nanoparticles with fullerene-like structure under shockwave pressures. *J. Am. Chem. Soc.* **127,** 16263–16272 (2005).
55. Joly-Pottuz, L. *et al.* Pressure-induced exfoliation of inorganic fullerene-like WS_2 particles in a Hertzian contact. *J. Appl. Phys.* **99,** 023524 (2006).

56. Bundy, F. P. The P, T phase and reaction diagram for elemental carbon. *J. Geophys. Res.* **85,** 6930–6936 (1979).
57. Krusin-Elbaum, L. *et al.* Room-temperature ferromagnetic nanotubes controlled by electron or hole doping. *Nature* **431,** 672–676 (2004).
58. Qian, L. *et al.* Improved optoelectronic characteristics of light-emitting diodes by using a dehydrated nanotube titanic acid (DNTA)-polymer nanocomposites. *J. Phys. Chem. B* **108,** 13928–13931 (2004).
59. Tokudome, H. & Miyauchi, M. Electrochromism of titanate-based nanotubes. *Angew. Chem. Int. Edn* **44,** 1974–1977 (2005).
60. Xu, X. G., Ding, X., Chen, Q. & Peng, L.-M. Electronic, optical, and magnetic properties of Fe-intercalated $H_2Ti_3O_7$ nanotubes: First-principles calculations and experiments. *Phys. Rev. B* **73,** 165403 (2006).
61. Liu, A., Wei, M., Honma, I. & Zhou, H. Biosensing properties of titanate-nanotube films: selective detection of dopamine in the presence of ascorbate and uric acid. *Adv. Funct. Mater.* **16,** 371–376 (2006).
62. Mor, G. K., Carvalho, M. A., Varghese, O. K., Pishko, M. V. & Grimes, C. A. A room-temperature TiO_2-nanotube hydrogen sensor able to self-clean photoactively from environmental contamination. *J. Mater. Res.* **19,** 628–634 (2004).
63. Ruan, C. M., Paulose, M., Vargese, O. K. & Grimes, C. A. Enhanced photoelectrochemical-response in highly ordered TiO_2 nanotube-arrays anodized in boric acid containing electrolyte. *Sol. Energ. Mater. Sol. Cell* **90,** 1283–1295 (2006).
64. Paulose, M.*et al.* Backside illuminated dye-sensitized solar cells based on titania nanotube array electrodes. *Nanotechnology* **17,** 1446–1448 (2006).
65. Paulose, M., Shankar, K., Varghese, O. K., Mor, G. K. & Grimes, C. A. Application of highly-ordered TiO_2 nanotube-arrays in heterojunction dye-sensitized solar cells. *J. Phys. D* **39,** 2498–2503 (2006).
66. Mitchell, D. T. *et al.* Smart nanotubes for bioseparations and biocatalysis. *J. Am. Chem. Soc.* **124,** 11864–11865 (2002).
67. Goldberger, J., Fan, R. & Yang, P. Inorganic nanotubes: A novel platform for nanofluidics. *Acc. Chem. Res.* **39,** 239–248 (2006).
68. Dhas, N. A. & Suslick, K. S. Sonochemical preparation of hollow nanospheres and nollow nanocrystals. *J. Am. Chem. Soc.* **127,** 2368–2369 (2005).
69. Cheng, F., Gou, X., Chen, J. & Xu, Q. Ni/MoS_2 nanocomposites as the catalysts for hydrodesulphurization of thiophene and thiophene derivatives. *Adv. Mater.* **18,** 2561–2564 (2006).
70. Chen, R., So, M. H., Yang, J., Deng, F., Chea, C. M. & Sun, H. Fabrication of bismuth subcarbonate nanotube arrays from bismuth citrate. *Chem. Commun.* 2265–2267 (2006).
71. Zhi, C., Bando, Y., Tang, C. & Golberg, D. Immobilization of proteins on BN nanotubes. *J. Am. Chem. Soc.* **127,** 17144–17145 (2005).
72. Chen, J., Li, S., Tao, Z., Shen, Y. & Cui, C. *J. Am. Chem. Soc.* **125,** 5284–5285 (2003).
73. Dominko, R. *et al. Electrochimica Acta* **48,** 3079–3084 (2003).
74. Li, J., Tang, Z. & Zhang, Z. H-titanate nanotube: a novel lithium intercalation host with large capacity and high rate capability. *Electrochem. Commun.* **7,** 62–67 (2005).
75. Li, W., Zhang, S. & Chen, J. Synthesis, characterization, and electrochemical application of $Ca(OH)_2$-, $Co(OH)_2$-, and $Y(OH)_3$-coated $Ni(OH)_2$ tubes. *J. Phys. Chem. B* **109,** 14025–14032 (2005).
76. Tenne, R. Issue 15 cover image. *Phys. Chem. Chem. Phys.* **6** (2004).

Acknowledgements

I am grateful to M. Bar-Sadan, I. Kaplan-Ashiri, R. Rosentsveig, A. Margolin, A, Albu-Yaron, R. Popovitz-Biro, S. R. Cohen, G. Seifert, M. Jansen, H. D. Wagner and J.M. Gordon for their help. The support of the Israeli Ministry of Science and Technology and the Israel Science Foundation is acknowledged.